High-bandwidth 3d force feedback optical tweezers for interactive bio-manipulation

Munan Yin, Edison Gerena, Cecile Pacoret, Sinan Haliyo, Stephane Regnier

High-bandwidth 3D Force Feedback Optical Tweezers for Interactive Bio-manipulation

Munan Yin[1†], Edison Gerena[1†], Cécile Pacoret[2], Sinan Haliyo[1] and Stéphane Régnier[1]

***Abstract*— Optical Tweezers are considered one of the most suitable techniques for biological tasks, however the lack of automation make this technology less accessible. We present here a new 3D force sensing method with high bandwidth (up to 10Khz) which can allow implementing complex robotic approaches. Proposed technique uses high speed image tracking with nano-metric resolution in 3 directions. Its capabilities are demonstrated in a teleoperated 3D manipulation scenario with a haptic user interface, where naive users performed direct *in vitro* haptic exploration of isolated Red Blood Cells inside a Petri dish.**

I. INTRODUCTION

Among a variety of microrobotic techniques, Optical Tweezers are considered to be one of the most suitable for biological characterization and manipulation [1], [2]. They consist on using the radiation pressure of a tightly focused laser beam to trap a micro-object in liquid solution [3]. The generated force can go up to few hundreds of pico-Newton. Although seemingly low, this is well in the range of micro-biological interactions and Optical Tweezers have successfully applied to a range of applications from sorting biological objects [4] to assembling complex micro-structures [5].

An inert, bio-compatible bead is generally used as a probe to avoid laser exposure to biological objects. Additionally, in this case the effect of the trap is akin to a linear stiffness around the focal point of the beam and the force acting on the object can be obtained by measuring its motion [6]. This particularity has led to the use of Optical Tweezers for force sensing, for example in mechanical characterization of molecular interactions [7] and of the cell membrane [8].

Current robotic research on Optical Tweezers focuses on the implementation of control techniques for automation [9], [10], [11] or teleoperation [12], [13], [14]. These works consider the trapped probe as the end-effector, and the external forces acting on the probe can be used in the feedback path to close the control loop. This forces can be provided by tracking the motion of the probe under the optical microscope. Considering the force range and the trap stiffness, pico-Newton resolution is reachable. This kind of performance would make Optical Tweezers a formidable apparatus for micromanipulation in general and for biology and biochemistry in particular. Nevertheless, high dynamics effects at the microscale and the limitations of the optical microscope render most classical algorithms useless. Hence, the lack of robust 3D tracking reduces most applications to simple planar tasks. Also, the latency and low bandwidth hurts the system stability and its real-time capabilities [15].

Several methods to improve the tracking has been developed. Most commonly, a quadrant photodiode (QDP) is used to sample the position of the target at tens of kHz with nanometric precision [16]. Nonetheless, this method is vulnerable to occlusions and disturbances and works reliably only on isolated objects. An alternative is image processing through video cameras integrated into the microscope. However, state-of-art real-time visual tracking algorithms on commercial CMOS cameras can rarely exceed 60 Hz [17]. Limiting the imaging to a smaller region of interest (ROI) can accelerate processing, at the detriment of resolution and precision [18]. By combining a high-speed CMOS with tracking implemented on GPUs (Graphics Processing Unit), 3D tracking at several of kHz is reported [19]. This approach is however fairly complex as it requires special knowledge and hardware.

As an alternative to classical CMOS cameras, silicon retina sensors were proposed [20]. These "asynchronous time-based image sensor"s are frame-free and eliminate data redundancy by design. They are shown to allow the 2D tracking at an unprecedented speed in the order of tens of kilo-Hertz [21]. Because of the particularity of the image data that they provide, well-known processing techniques cannot be used. Further investigations are especially needed for real-time 3D robust tracking.

We present here a 3D motion tracking technique using an event-based algorithm taking advantage of a silicon retina sensor. It provides pico-Newton resolution and its bandwidth reaches 10 kHz. Its capabilities are demonstrated in a teleoperated 3D manipulation scenario with a haptic user interface. This kind of control scheme is very demanding and requires indeed a feedback loop at 1 kHz for stability.

II. 3D HIGH-SPEED FORCE SENSING

A. System Description

The optical scheme of the system is shown in Fig.1 (a). It's based on an inverted microscope where the same objective is used for both imaging and producing the optical trap. Its singularity is to include an ATIS, "asynchronous time-based

† These authors contributed equally to this work.

*This work was supported by the French National Research Agency through the ANR-IOTA project (ANR-16-CE33-0002-01), and partially by the French government research program "Investissements d'avenir" through the Robotex Equipment of Excellence (ANR-10-EQPX-44).

[1]M. Yin, E. Gerena, S. Haliyo and S. Régnier are with the Sorbonne Universités, UPMC Univ Paris 06, CNRS, Institut des Systèmes Intelligents et de Robotique UMR 722, 4 place Jussieu, 75005 Paris, France. {yin,gerena,haliyo,regnier}@isir.upmc.fr

[2]C. Pacoret is with the University of Geneva, Department of Basic Neurosciences, Campus Biotech, 9 Chemin des Mines, 1205 Geneva, Switzerland. cecile.pacoret@unige.ch

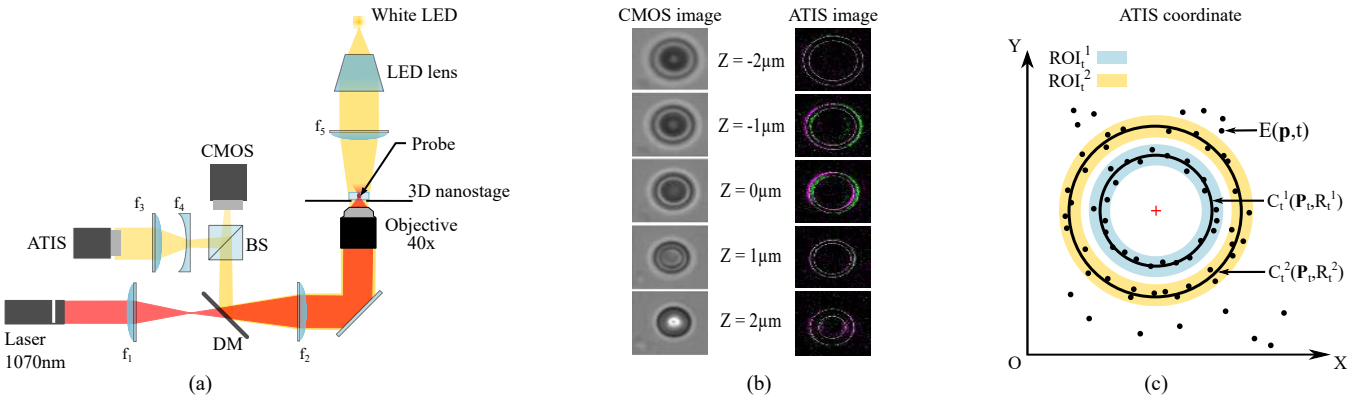

Fig. 1. (a) Optical scheme. The source is a 1070 nm laser with a maximum output of 10 Watts. An oil immersion objective (Olympus UPlanFLN 40x, NA 1.3) produces a fixed optical trap. Two microstages (x - y) and a 3D nanostage provide respectively coarse and fine positioning of samples. The illumination(LED, 3W) is reflected by a long pass dichroic mirror (900nm cut-off) then is divided by an unpolarized beam splitter (R9:T1) into the silicon retina camera (ATIS, 240×304 pixels) and the CMOS camera (Basler, 659×494 pixels) $f_1 = 30, f_2 = 125, f_3 = 100, f_4 = -50, f_5 = 45$, (b) Image of microbead (3μm polystyrene) under the system. First column: the CMOS image at different z-displacements respect to the focus plane (z=0). Second column: the corresponding ATIS image with 33 ms accumulation time. Different colors indicate positive or negative polarity of the events. The displacements are in μm. (c) Working principle of the event-based ring tracking algorithm.

image sensor" silicon retina. ATIS has the particularity to be adaptable to high-speed on-line tracking due to its efficient encoding of movements, as the data redundancy is eliminated by design. Each pixel is electronically independent and generate events immediately when a light variation above a threshold is detected. This data is asynchronous and an event may have positive or negative polarity. More details of this technology are discussed in [22], [23].

In a scene with the stable light environment, only the dynamic information stimulated by moving object is recorded. In the case of the presented system, the trap center has a fixed position in the ATIS image. With an appropriate threshold, image variations are mostly generated on the contour of the trapped bead as shown in Fig.1 (b). This information is exploited to infer the 3D motion of the probe.

B. 3D Tracking

Fig.1 (b) shows the conventional and event-based images of the probe. In ATIS image, accumulated events can be grouped in two concentric circles. Their center position is related to the planar motion of the probe while the radius is linked to the depth position. An event-based ring tracking algorithm is developed. It's used to recognize both circles, then to selectively extract center position and radius parameters from the inner one. Indeed, when the probe is in contact with other samples, the inner one is much more robust and stable. However, it's necessary to track both circles to be able to set them apart. The principle of ring tracking is to minimize the distance of the events' spatial coordinates and the ring model [24] as presented in Fig.1 (c).

Denoting $\mathbf{E}(\mathbf{p}, t)$ as an event occurs at time t with spatial location $\mathbf{p} = (x, y)$ in ATIS coordinate. $U(t)$ is defined as the set of useful events' locations at time t:

$$U(t) = \{\mathbf{E}(\mathbf{p}, t) | \mathbf{p} \in ROI(t)\} \tag{1}$$

where $ROI(t)$ is the region of interest (ROI) of one circle model at time t [25]. Since the fitting methods are vulnerable to noise, the ROI is used as solution to filter the outliers.

Suppose that the unknown circle model's parameters at time t is $\mathbf{C_t}(\mathbf{P_t}, R_t)$, where $\mathbf{P_t} = (X_t, Y_t)$ is the circle center's position and R_t is the radius. Then, a fast non-iterative algebraic fit [26] minimizes the cost function:

$$\min_{\mathbf{P_t} \in \mathbb{R}^2 R_t \in \mathbb{R}} \sum_{\mathbf{p_k} \in U(t)} \| d(\mathbf{p_k}, \mathbf{P_t})^2 - R_t^2 \|^2 \tag{2}$$

where $\mathbf{p_k}$ is the kth event's location in $U(t)$. $d(\mathbf{p_k}, \mathbf{P_t})$ is Euclidean distance between $\mathbf{p_k}$ and the circle center $\mathbf{P_t}$. Introducing parameters $A = -2X_t$, $B = -2Y_t$, and $C = {X_t}^2 + {Y_t}^2 - {R_t}^2$, (2) can be written as a linear least square problem:

$$\min_{\mathbf{P_t} \in \mathbb{R}^2 R_t \in \mathbb{R}} \sum_{\mathbf{p_k} \in U(t)} \| Ax_k + By_k + C + {x_k}^2 + {y_k}^2 \|^2 \tag{3}$$

Solving A, B, and C, gives the parameters of circle $(\mathbf{P_t}, R_t)$. This single circle tracking method is used to parametrize the two concentric circles of the ring (inner $\mathbf{C_t^1}$ and outer $\mathbf{C_t^2}$). All incoming event occurring in a considered time interval are assigned to the closest circle model. Events at the intersection of two ROIs are discarded to reduce the ambiguity. This condition makes sure that the inner and outer circle will not become into one. The ROIs are updated accordingly. The algorithm is given below.

Algorithm 1 Event-based Robust Ring Fitting

Require : Events $\mathbf{E}(\mathbf{p}, t)$

1: **for** every *step* **do**
2: Update the content of $\mathbf{U^1(t)}$ and $\mathbf{U^2(t)}$ according to (1)
3: Estimate $\mathbf{C_t^1}$ and $\mathbf{C_t^2}$ parameters according to (3).
4: Update output : $[\mathbf{X_t^1}, \mathbf{Y_t^1}, \mathbf{R_t^1}]$
5: Update $\mathbf{ROI_{t+1}^1}$ and $\mathbf{ROI_{t+1}^2}$
6: **end for**

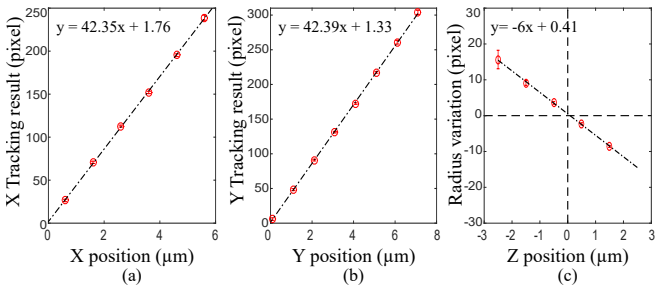

Fig. 2. The 3D detection range of the system. (a), (b) The inner center position x and y (in pixels) with the microsphere's position (in μm). (c) The relative inner radii change (in pixels) with the microsphere's axial position (in μm). At focus plane, the inner radius is 64 pixels. The linear regression coefficients show the conversion between pixels in ATIS coordinates and micrometers in the world coordinates.

C. Evaluation of tracking

1) Range and resolution: A 3 μm silica microsphere fixed to the sample-holder is used to evaluate the tracking. Fig.2 gives the real displacement, as reported by the nanostage vs tracked motion in pixels for all directions as well as the calculated pixel/μm transform.

The detectable motion range is 6μm and 7μm for x and y respectively with less than 3% standard deviation (SD). On z-axis, the relative radii variance is shown in Fig.2 (c). The linear detection range is about ± 2 μm around the focus plane with 5 % SD. This 3D detection range ($6 \times 7 \times 4\mu$m) is sufficient since the linearity of the trap stiffness is valid around one diameter of the trapped bead [6], here $3 \times 3 \times 3\mu m^3$.

With 204×304 pixels, the theoretical resolution is 23.8nm/pixel in x and y and 166.6 nm/pixel in z. Practically, the bead center position and radius were estimated with sub-pixel accuracy using the circle tracking algorithm. This sensitivity varies in different illumination conditions and working environment.

2) Robustness: Robustness here is defined as the ability to extract the 3D position of the target from noisy data, or even a small subset of data. It will be tested under two most commonly encountered situations partial occlusion i.e. only part of the target image is captured, and obstacles disturbances i.e. to track the target among many obstacles.

In the occlusion test, the microsphere's image is partially out of the view of ATIS. The tracking errors for 30% occlusion of the inner circle are shown in Fig.3(c). As can be seen, for less than 30% occlusion, the tracking error and the SD are less than 5% for both lateral and axial detection.

In obstacles disturbance test, the target bead (in the center) is surrounded by two other similar objects as shown in Fig.3 (d). They are fixed on Petri-dish and animated with a sinusoidal movement. The tracking result is shown in Fig.3 (f). The lateral tracking errors are less than $\pm$5% with 2% SD in within ± 2.5 μm. The axial errors are less than $\pm$ 20 % around the focus plane with less than 10 % SD. As the image plane move far away from focus plane, the radius error increases up to 30 %.

3) Computational Load: The algorithm is implemented in C++ on a hard real-time framework. The testing relies on a 2.9 GHz Dual core desktop PC, with a total CPU load about 50 % of its power and a memory consumption of about 4 MB. The average running time for each iteration is less than 60 μs, with less than 2 μs deviation. Then the system is successfully pushed to 10 kHz real-time sampling rate.

III. 3D HAPTIC FEEDBACK OPTICAL TWEEZERS

A. Haptic Coupling

In order to show its benefits and validate the proposed force sensing, a teleopration scenario with haptic feedback is implemented. This is a demanding application from the control point of view as the stability and transparency of haptic feedback coupling requires a sampling of 1 kHz [27], [15]. Previous works presented haptic feedback on Optical

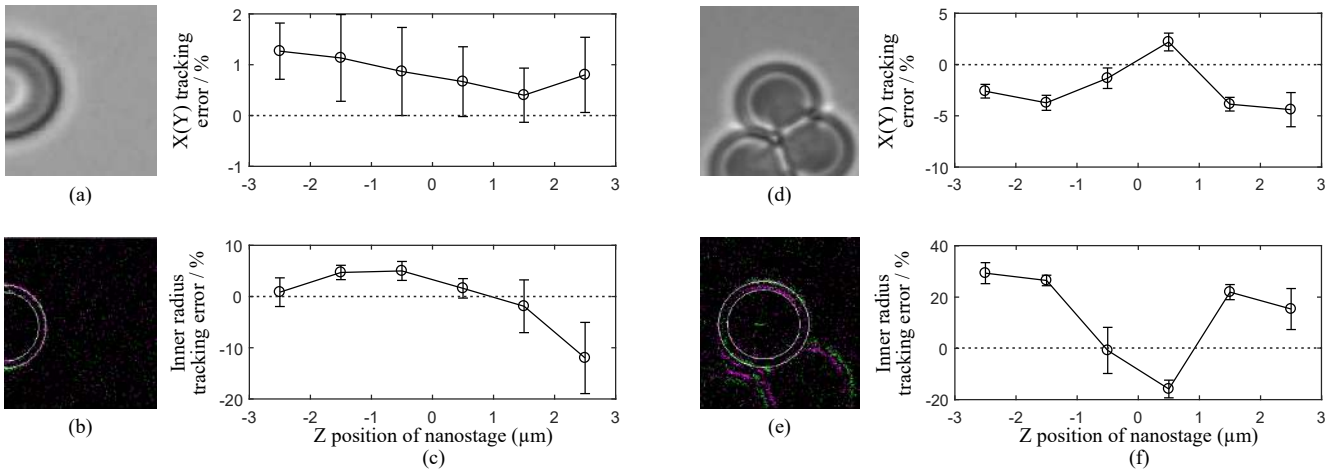

Fig. 3. Robustness tests. (a), (b) and (c) Robustness under 30% partial occlusion situation. (d), (e) and (f) Robustness in obstacles disturbance situation. (a) and (d) Image recorded by the CMOS camera. (b) and (e) Corresponding image recorded by ATIS with accumulation time of 33 ms. (c) and (f) The mean and SD of the tracking error during each test. The tracking error is determined as the difference between the detection and the ground truth, divided by the detection range in corresponding axis.

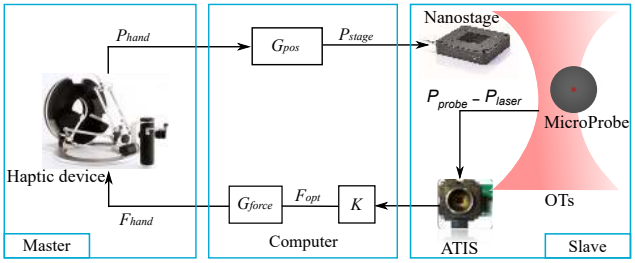

Fig. 4. The schematic diagram of the bilateral coupling of the position and force in the haptic OTs system.

Tweezers but were limited to 2D [13], [14]. The 3D tracking allows for a real spatial coupling in this case.

Haptic feedback requires a bilateral control scheme, as presented in Fig.4. In this scheme, the user handles the haptic interface (Omega.7, ForceDimension). Its position is used to control the motion of the sample through the nano-stage. The force measured on the probe is feedback to the user with an appropriate gain.

Motion of the master device is scaled down by 6×10^{-4} to drive the trap position relatively to sample holder. Actually, the trap position is fixed, and the mobile part is the nanostage holding the samples. Nano-stage can be driven in two modes, rate-control to cover the whole working space (200×200 μm), and position-control to execute precise tasks. The measured forces are magnified by 1×10^{12} and sent back to the user. The force on the trap is calculated using the optical force model [6] :

$$\mathbf{F}_{opt} = \mathbf{K} \times (\mathbf{P}_{laser} - \mathbf{P}_{probe}) \quad (4)$$

where $\mathbf{P}_{laser} - \mathbf{P}_{probe}$ represent the displacement between the laser and the probe position as obtained from the tracking method. $\mathbf{K}$ is the stiffness of the trap. This stiffness can be calculated experimentally using the Equipartition method [28]. Considering 30 mW laser power it is estimated in x-axis, y-axis and z-axis as K_x=12.3 pN/μm, K_y=12.6 pN/μm s and K_z=1.5 pN/μm respectively under room temperature of 25.5 $^\circ C$.

A single PC (Intel Xeon core, 2.93 GHz) operating under a real-time co-kernel Linux and RTOS APIs Xenomai is used to control the system. The control-loop runs with a force refresh rate of 1 kHz.

TABLE I

SUMMARY OF SYSTEM PARAMETERS

OTs stiffness (pN/μm)	x= 12.3	y= 12.6	z= 1.5
Force detection range (pN)	x= 36.9	y= 37.8	z= 4.5
Force resolution (pN)	x= 0.3	y= 0.3	z= 0.25
Haptic loop	1 kHz hard real-time		

B. 3D Haptic Experiments on biologic samples

Biologic samples are chosen to illustrate the use of the system in a real world scenario. Red Blood Cells (RBC) are easy to acquire and have an 3D irregular dumbbell-shaped profile, and hence are well suited for this illustration. They are fixed in 4% formaldehyde for biological stability. Probes are 3μm polystyrene beads incubated in PBS and Ethylenediaminetetraacetic acid (EDTA) solution to prevent the surface sticking.

1) z-axis Haptic Feedback: The first experiment will validate the force feedback on z axis. The RBC sample is fixed on the bottom of a Petri Dish. The user first traps a bead to serve as probe, then moves the sample-holder as to position the probe above a fixed RBC. The planar motion of the nanostage is then artificially blocked and the user controls only the z motion until the probe touches the cell and he feels an obvious counter-force. The experimental results are shown in Figure 5.A. Small fluctuations are caused by the 3D Brownian motion of probe which are largely present at the considered scale. The contact point is shown in region II in (a), (b), (c). At contact, a sudden reaction force in the z-axis of about 0.3 pN is detected, and the Brownian motion is attenuated compared to the region I. Then the probe is pushed deeper into the cell until 1.6 pN in the z-direction, as shown in III. At this time, user felt about 1.6 N force in the z-axis. The cell is contacted twice during the presented experiment. Similar results are obtained during the two passes which also proves the repeatability of the axial force detection.

Notice that this experiment aims to validate the axial haptic feedback during biological manipulations. In addition, the stiffness of the RBCs can be roughly obtained from the result. By using the Hertz model, which considers the cell a homogeneous smooth semi-sphere, the elastic modulus of the RBC is calculated as 33.7 Pa [29]. This result is similar to literature, with the measure of the elastic modulus of adherent living cells [30]. This is an approximated result; for a proper mechanical characterization, the trap stiffness should be calibrated in the neighborhood of the cell before [31]. The system would also allow to automatize the experiment and to repeat it accurately over a large number of trials.

2) 3D Haptic Exploration: This experiment is dedicated to touch the 3D contour of cells and explore their shapes. The difficulty of these tasks comes from the uncertainty contour of the biological objects. Since the visual information may be blurry or lost at some parts, the haptic feedback will help users to maintain the contact and decrease the possibility of losing the trap.

This experiment is dedicated to let a user touch the 3D contour of cells and explore their shapes. The difficulty of these tasks comes from the uncertainty and irregularity of biological objects. Since the visual information is blurry and lacks the depth of field, and the probe is eventually occluded by the sample itself, the haptic feedback would help to maintain the contact.

First, 2 flat and transparent RBCs, damaged after the hemoglobin leakage, stuck together forming a ∞ shape is explored (fig. 5.B). Another experiment is conducted on a isolated RBC (fig. 5.C). The 3D contact force is successfully perceived and maintained by operators. Haptic feedback allows to keep the contact even when the probe is occluded and users were able to achieve a surface exploration with consistent force feedback.

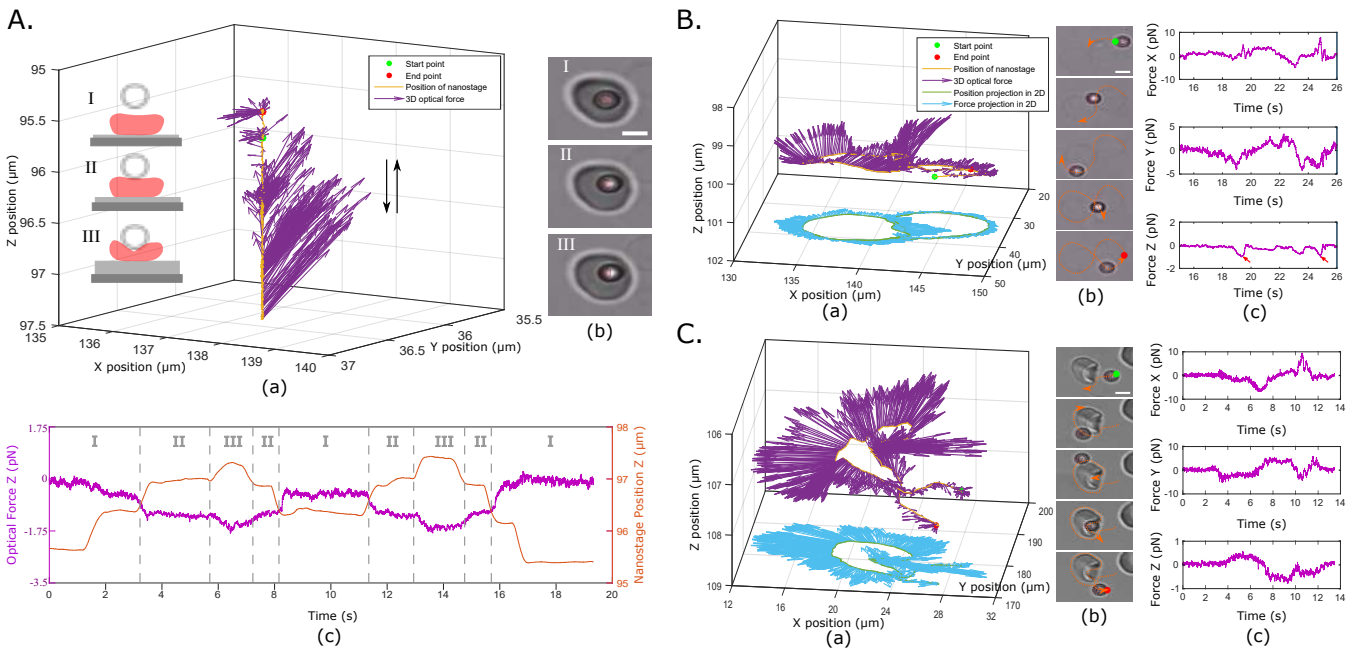

Fig. 5. 3D Haptic micro biological experiment **A.** Pressing on a Red Blood Cell from above. (a) The 3D force applied on the probe during the experiment. The *x*-, *y*-, *z*- coordinates are the position of nanostage in world coordinates. inset picture I: the optically trapped probe is not in contact with the cell; II: by increasing the position of the nanostage, the probe is coming into contact with the RBC; III: the probe pushes deeper into the RBC. (b) Pictures of RBC and the probe corresponding to the three stages I, II, III. (c) The optical force and the position of nanostage in *z*-direction during the cell pressing process. **B.** Exploration of two connected transparent RBCs. (a) The 3D path of probe and 3D contact forces during the contour exploration. (b) Corresponding pictures under microscope during this process. (c) 3D optical force. When the probe pass through the connected part of two cells, a burst of axial force of 1 pN is detected (red arrow). **C.** Touch the contour of a RBC using the probe. (a) The 3D path of the probe and the 3D contact forces during the RBC contour exploration. (b) Pictures of this process under microscopy. (c) 3D optical force during this process. The scale bars are 3 μm.

3) Preliminary user evaluations: To further prove the repeatability and effectiveness of the 3D haptic feedback during biological manipulations, a preliminary users study is conducted. 6 volunteers explored the shape of one identical RBC. Each were subject to those three different conditions: with only vision feedback, both vision and haptic feedback, and only haptic feedback respectively. Before the formal evaluation, the participants were trained to use the system for about 10 minutes and shown how to trap microbeads to serve as probes. They were than asked to roll the probe around the cell while keeping the contact at all times. The task under each condition was conducted twice. The probe trajectory during three users' experiments are depicted in Fig. 6 (a), (b) and (c).

During this experiment, it is observed that exploration with only haptic information is time-consuming. Users are required more to concentrate on the force feedback hence move slowly. Full exploration is successfully completed only in half of the trials. Due to the lack of vision information, the users can hardly estimate the path to follow. With only vision feedback, users frequently lose the trapped object (33%) because of large contact forces difficult to infer from vision alone. This is also probably caused by some shadows and invisible features that are barely noticed.

Combining the haptic feedback and vision overcomes the above shortages. Vision provides general overview information of the scene and haptic feedback allows for fine control skills. The haptic feedback largely decreases the rate of losing trap to 17% and users performs the task more efficiently. Note however that this is a preliminary qualitative analysis. A formal user evaluation comparing both modalities is planned.

IV. CONCLUSION AND FUTURE WORK

We have presented a new method for 3D force sensing for Optical Tweezers, with high bandwidth (up to 10Khz), in a large three-dimensional workspace that covers the full linear domain of a single trapped bead and pico-newton sensibility with a theoretical resolution of 0,3pN. The force sensing is based on high-speed optical processing implemented through a silicon retina and its dedicated tracking algorithm.

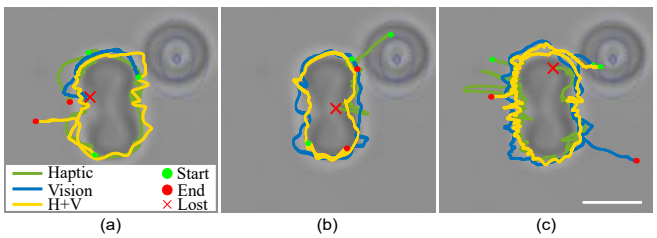

Fig. 6. The trajectories of the probe during the experiment of RBC surface exploration. (a), (b), (c) The result of three participants under different experiment conditions: touching with only visual feedback, only haptic feedback, and both haptic and visual feedback are shown in green, blue, and yellow respectively. The red cross indicates that the user has lost the trapped probe during the experiment. The scale bar is 3 μm

Thanks to the capabilities of force sensing, and because of the stable and simple set-up design, complex tasks have been demonstrated in real biological environment on a haptic teleoperation platform. This is a good illustration of the kind of new robotic application that can benefit from the proposed 3D sensing. A simple user study has shown that non-expert user can take in hand the optical tweezers after few minutes of training. It is safe to assume that expert user will be able to perform complex tasks more efficiently.

The real-time particle-tracking scheme can be also extended to magnetic tweezers and other micro-robotics techniques. The method remains compatible with fluorescence, interferential and superresolution microscopy. An interesting development would be a Scanning Force Microscopy technique adapted to biological environments.

In future works, we plan to extend this fast 3D force sensing capabilities to several trapped objects. Current state-of-the-art of multi-trap optical tweezers usually do not include force sensing capabilities [32]. Multi-trap optical tweezers or optically actuated microtools [33] with highly transparent force feedback will be advantageous for numerous biomedical applications.

REFERENCES

[1] J. R. Moffitt, Y. R. Chemla, S. B. Smith, and C. Bustamante, "Recent advances in optical tweezers," *Biochemistry*, vol. 77, no. 1, p. 205, 2008.

[2] F. M. Fazal and S. M. Block, "Optical tweezers study life under tension," *Nature photonics*, vol. 5, no. 6, pp. 318–321, 2011.

[3] A. Ashkin, J. Dziedzic, and T. Yamane, "Optical trapping and manipulation of single cells using infrared laser beams," *Nature*, vol. 330, no. 6150, pp. 769–771, 1987.

[4] S. Grover, A. Skirtach, R. Gauthier, and C. Grover, "Automated single-cell sorting system based on optical trapping," *Journal of biomedical optics*, vol. 6, no. 1, pp. 14–22, 2001.

[5] G. Akselrod, W. Timp, U. Mirsaidov, Q. Zhao, C. Li, R. Timp, K. Timp, P. Matsudaira, and G. Timp, "Laser-guided assembly of heterotypic three-dimensional living cell microarrays," *Biophysical journal*, vol. 91, no. 9, pp. 3465–3473, 2006.

[6] A. Ashkin, "Forces of a single-beam gradient laser trap on a dielectric sphere in the ray optics regime," *Biophysical journal*, vol. 61, no. 2, p. 569, 1992.

[7] A. L. Stout, "Detection and characterization of individual intermolecular bonds using optical tweezers," *Biophysical journal*, vol. 80, no. 6, pp. 2976–2986, 2001.

[8] D. Raucher and M. P. Sheetz, "Characteristics of a membrane reservoir buffering membrane tension," *Biophysical journal*, vol. 77, no. 4, pp. 1992–2002, 1999.

[9] D. Sun and H. Chen, "Moving groups of microparticles into array with a robot–tweezers manipulation system," *IEEE Transactions on Robotics*, vol. 28, no. 5, pp. 1069–1080, 2012.

[10] A. G. Banerjee, S. Chowdhury, W. Losert, and S. K. Gupta, "Real-time path planning for coordinated transport of multiple particles using optical tweezers," *IEEE Transactions on Automation Science and Engineering*, vol. 9, no. 4, pp. 669–678, 2012.

[11] D. Sun, X. Li, C. C. Cheah, and S. Hu, "Dynamic trapping and manipulation of biological cells with optical tweezers," *Automatica*, vol. 49, no. 6, pp. 1614–1625, 2013.

[12] C. Pacoret, R. Bowman, G. Gibson, S. Haliyo, D. Carberry, A. Bergander, S. Régnier, and M. Padgett, "Touching the microworld with force-feedback optical tweezers," *Optics express*, vol. 17, no. 12, pp. 10 259–10 264, 2009.

[13] Z. Ni, A. Bolopion, J. Agnus, R. Benosman, and S. Régnier, "Asynchronous event-based visual shape tracking for stable haptic feedback in microrobotics," *IEEE Transactions on Robotics*, vol. 28, no. 5, pp. 1081–1089, 2012.

[14] K. Onda and F. Arai, "Multi-beam bilateral teleoperation of holographic optical tweezers," *Optics express*, vol. 20, no. 4, pp. 3633–3641, 2012.

[15] A. Bolopion, B. Cagneau, D. S. Haliyo, and S. Régnier, "Analysis of stability and transparency for nanoscale force feedback in bilateral coupling," *Journal of Micro-Nano Mechatronics*, vol. 4, no. 4, p. 145, 2008.

[16] D. Ruh, B. Tränkle, and A. Rohrbach, "Fast parallel interferometric 3d tracking of numerous optically trapped particles and their hydrodynamic interaction," *Optics express*, vol. 19, no. 22, pp. 21 627–21 642, 2011.

[17] A. Handa, R. A. Newcombe, A. Angeli, and A. J. Davison, "Real-time camera tracking: When is high frame-rate best?" in *Computer Vision–ECCV 2012*. Springer, 2012, pp. 222–235.

[18] R. Bowman, D. Preece, G. Gibson, and M. Padgett, "Stereoscopic particle tracking for 3d touch, vision and closed-loop control in optical tweezers," *Journal of optics*, vol. 13, no. 4, p. 044003, 2011.

[19] A. Huhle, D. Klaue, H. Brutzer, P. Daldrop, S. Joo, O. Otto, U. F. Keyser, and R. Seidel, "Camera-based three-dimensional real-time particle tracking at khz rates and ångström accuracy," *Nature communications*, vol. 6, 2015.

[20] Z. Ni, C. Pacoret, R. Benosman, and S. Régnier, "2d high speed force feedback teleoperation of optical tweezers," in *Robotics and Automation (ICRA), 2013 IEEE International Conference on*. IEEE, 2013, pp. 1700–1705.

[21] Z. Ni, A. Bolopion, J. Agnus, R. Benosman, and S. Régnier, "Asynchronous event-based visual shape tracking for stable haptic feedback in microrobotics," *IEEE Transactions on Robotics*, vol. 28, no. 5, pp. 1081–1089, 2012.

[22] C. Posch, D. Matolin, and R. Wohlgenannt, "A qvga 143 db dynamic range frame-free pwm image sensor with lossless pixel-level video compression and time-domain cds," *Solid-State Circuits, IEEE Journal of*, vol. 46, no. 1, pp. 259–275, 2011.

[23] C. Posch and D. Matolin, "Sensitivity and uniformity of a 0.18μm cmos temporal contrast pixel array," in *2011 IEEE International Symposium of Circuits and Systems (ISCAS)*. IEEE, 2011, pp. 1572–1575.

[24] W. Gander, G. H. Golub, and R. Strebel, "Least-squares fitting of circles and ellipses," *BIT Numerical Mathematics*, vol. 34, no. 4, pp. 558–578, 1994.

[25] P. J. Huber, *Robust statistics*. Springer, 2011.

[26] I. Kåsa, "A circle fitting procedure and its error analysis," *IEEE Transactions on instrumentation and measurement*, vol. 1001, no. 1, pp. 8–14, 1976.

[27] R. T. Verrillo, "Effect of contactor area on the vibrotactile threshold," *The Journal of the Acoustical Society of America*, vol. 35, no. 12, pp. 1962–1966, 1963.

[28] K. C. Neuman and S. M. Block, "Optical trapping," *Review of scientific instruments*, vol. 75, no. 9, pp. 2787–2809, 2004.

[29] N. Guz, M. Dokukin, V. Kalaparthi, and I. Sokolov, "If cell mechanics can be described by elastic modulus: study of different models and probes used in indentation experiments," *Biophysical journal*, vol. 107, no. 3, pp. 564–575, 2014.

[30] E. Planus, R. Fodil, M. Balland, D. Isabey *et al.*, "Assessment of mechanical properties of adherent living cells by bead micromanipulation: comparison of magnetic twisting cytometry vs optical tweezers," *Journal of biomechanical engineering*, vol. 124, no. 4, pp. 408–421, 2002.

[31] S. Nawaz, P. Sánchez, K. Bodensiek, S. Li, M. Simons, and I. A. Schaap, "Cell visco-elasticity measured with afm and optical trapping at sub-micrometer deformations," *PLoS One*, vol. 7, no. 9, p. e45297, 2012.

[32] D. G. Grier, "A revolution in optical manipulation," *Nature*, vol. 424, no. 6950, pp. 810–816, 2003.

[33] M. J. Villangca, D. Palima, A. R. Bañas, and J. Glückstad, "Light-driven micro-tool equipped with a syringe function," *Light: Science & Applications*, vol. 5, no. 9, p. e16148, 2016.